Photocatalytic robust solar energy reduction of dinitrogen to ammonia on ultrathin MoS_2

Songmei Sun [1], Xiaoman Li [1], Wenzhong Wang [*], Ling Zhang, Xiang Sun

State Key Laboratory of High Performance Ceramics and Superfine Microstructure, Shanghai Institute of Ceramics, Chinese Academy of Sciences, Shanghai 200050, PR China

article info

Keywords:
Photocatalysis
N_2 reduction
Solar energy conversion
Ultrathin material

abstract

The crux for solar N_2 reduction to ammonia is activating N_2 into its high-energy intermediate. Apply-ing a simultaneous multi-electron reduction process could avoid intermediate generation and decrease the thermodynamic barrier. However, this process is extremely difficult from a kinetic view and exper-iments so far have not shown it is accessible. Here we show the first direct evidence of trion induced multi-electron N_2 reduction on ultrathin MoS_2 . By applying light induced trions, N_2 molecular was acti-vated and transformed into ammonia by a simultaneous six-electron reduction process, with a high ammonia synthesis rate of 325 mol/g h without the assistant of any organic scavengers or co-catalyst. Bulk MoS_2 without trions did not exhibit any activity. This demonstrates multi-electron reduction may be realized in electron-rich semiconductors with high concentration of localized electrons such as trions. The methodology of simultaneous multi-electron reduction has wide implications for reactions beyond N_2 reduction and for materials beyond MoS_2 .

1. Introduction

Heterogeneous catalytic conversion of N_2 to ammonia is one of the most important reactions in science and technology. It has played an important role in the development of modern industry and agriculture. Molecular N_2 is chemically and biologically inert due to its extremely strong, nonpolar triple bond (225 kcal/mol) as well as the large ionization potential [1–3]. The industrial ammo-nia synthesis typified by the Haber-Bosch process requires drastic reaction conditions of high pressures and temperatures [1,2,4,5], consuming 1–2% of the world's power source and generating more than 300 million tons of carbon dioxide [6]. Since the discovery of the first UV light induced N_2 reduction on TiO_2 based semicon-ductors by Schrauzer and Guth in 1977 [7], a great deal of efforts have been devoted to develop this green and economical ammonia synthesis routes that are capable of working under mild conditions.

Up to the present, various semiconductor photocatalysts, such as TiO_2 , WO_3 , $Sm_2O_3 \cdot nH_2O$ / $V_2O_3 \cdot nH_2O$ and diamond etc., have been reported which could convert atmospheric N_2 to ammonia under UV or visible light irradiation [8–13]. However, the obtained ammonia concentrations by most of these photocatalysts were only in the M magnitude [8–13], which is far away from the practi-cal demand. This dissatisfactory ammonia yield mainly arises from the difficult activation of insert N_2 on these catalysts, which is an uphill reaction process involved the generation of high-energy intermediate (N_2H, N_2H_2) [14–16]. For example, the reduction potential of the N_2H formation is as negative as −3.2 V vs. NHE via $N_2 + H^+ + e^- \rightarrow N_2H$. Through a two electron reduction process via $N_2 + 2H_2O + 4H^+ + 2e^- \rightarrow 2NH_3OH^+$, the reduction potential (-1.83 V vs. NHE) is still energetically impossible for most of traditional semiconductors (TiO_2 , WO_3 , Fe_2O_3 , ZnO etc.) in the absence of any organic scavengers or precious-metal cocatalysts. Applying a multi-electron reduction process via $N_2 + 5H^+ + 4e^- \rightarrow N_2H_5^+$ (-0.23 V vs. NHE) or $N_2 + 8H^+ + 6e^- \rightarrow 2NH_4^+$ (0.274 V vs. NHE), in principle, may avoid the generation of high energy intermediates and decrease the thermodynamic barrier for ammonia production. However, this multi-electron photoreduction of N_2 is extremely difficult from a kinetic point and has not been reported accessible up to the present. Recently, Zhang et al. found localized electrons in oxygen vacancy could effectively active the adsorbed N_2 by electron donation and decrease the kinetic barrier for N_2 photoreduction [17]. Kitano et al. reported Ru-loaded electride $[Ca_{24}Al_{28}O_{64}]^{4+}(e^-)_4$ (Ru/C12A7:e^-), which has high electron-donating power, works as an efficient cata-lyst for industrial ammonia synthesis [18]. These studies imply the unique advantage of electron-rich systems for N_2 activation and

* Corresponding author.
E-mail address: wzwang@mail.sic.ac.cn (W. Wang).
[1] Both these authors contributed equally to this work.

reduction. Multi-electron N_2 reduction may be realized by increas-ing the concentration of localized electrons in a semiconductor.

To achieve this important goal, ultrathin transition metal dichalcogenides (TMDs) (e.g., MoS_2 , $MoSe_2$, WS_2 , WSe_2) with intriguing electrical, optical, and photovoltaic performances [19–22], were chosen as model materials. It has been reported the photoexcited electron-hole pairs in ultrathin TMDs could form tightly bound excitons [23–27]. Gedik et al. proved these tightly bound excitons can capture additional electrons to form charged excitons (such as trions) which possess exceptionally high disso-ciation energies (20–50 meV) [28]. These charged excitons with more than two electron in one bound state may act as electron-rich species to facilitate multi-electron reduction process of molecu-lar N_2 . Although TMDs have been widely used as electrocatalytic material for hydrogen evolution [29–31], the influence and impli-cations of charged excitons for catalytic applications have not been explored thus far. Herein, we report the first experimental con-firmation of photocatalytic N_2 reduction to ammonia by charged excitons on ultrathin MoS_2 . The effect of charged excitons on the optical, optoelectronic, and electrochemical properties that signifi-cantly influence the photocatalytic N_2 reduction performance were discussed detailed in this manuscript.

2. Experimental section

2.1. Chemicals

All the chemical reagents were of analytical purity and were used as received from Shanghai Chemical Company without further purification.

2.2. Preparation

Hydrothermal MoS_2 was prepared by a previously reported method [32]. Typically, 7 mmol sodium molybdate dihydrate ($Na_2MoO_4 \cdot 2H_2O$) and 35 mmol thiourea (Mo:S = 1:5) were dis-solved in 40 mL distilled water under vigorous stirring to form a homogeneous solution, then the pH was adjusted to less than 1 with 2 M HCl. After being stirred for 30 min, the solution was transferred into a 45 mL Teflon-lined stainless steel autoclave, maintained at 200 ° C for 24 h and allowed to cool down to room temperature naturally. The obtained products were collected by centrifugation, washed with distilled water and ethanol, and dried at 60 ° C about 12 h.

Sonicated ultrathin MoS_2 was prepared by ultrasonic treatment of the hydrothermal MoS_2 in water for 12 h. The obtained disper-sion was centrifuged at a speed of 7000 rpm for 10 min. The top suspension was collected and freeze-drying to obtain the final son-icated ultrathin MoS_2 .

2.3. Characterization

The purity and the crystallinity of the as-prepared samples were characterized by powder X-ray diffraction (XRD) on a Japan Rigaku Rotaflex diffractometer using Cu K radiation while the voltage and electric current were held at 40 kV and 100 mA. The transmission electron microscope (TEM) analyses were per-formed by a JEOL JEM- 2100 F field emission electron microscope. UV–vis diffuse reflectance spectra (DRS) of the samples were measured using a Hitachi UV-3010PC UV–vis spectrophotome-ter. The photoluminescence (PL) spectra were measured with a Hitachi F4600 fluorescence spectrophotometer (excitation wave-length = 340 nm). Fourier transform infrared (FTIR) spectrum of concentrated ammonia product was performed with a spectropho-tometer (Nicolet 380, Thermo, USA). Ion chromatography was measured using THERMO FISHER ICS-2100 Ion Chromatography System. Inductively coupled plasma-atomic emission spectrometry (ICP-AES) was performed on Agilent 725.

2.4. Photocatalytic test

Simulated solar light induced N_2 reduction experiments were performed under a 500 W Xe lamp located approximately 10 cm from the sample. Visible light was provided under this Xe lamp with a 420 nm cutoff filter. The reaction cell was made of Pyrex glass with a quartz window on top. For the atmospheric N_2 fixation, 0.015 g of the as-prepared photocatalyst powder was dispersed in 200 mL deionized water and then stirring under the simulated solar light irradiation. For ^{15}N isotopic labelling experiment, the reaction cell was enclosed by a quartz window on top. N_2 (20% $^{15}N_2$, 80% $^{14}N_2$) gas was slowly bubbled through the reaction vessel, which con-tained 200 mL deionized water until that was saturated. Then the reaction vessel was sealed and irradiated under the simulated solar light irradiation. During the photocatalytic tests, the temperature of the reaction vessel was maintained at 25 ° C by providing a flow of cooling water. The concentration of ammonia in the reactor solu-tion was measured using the indophenol blue method. The amount of evolved O_2 was determined by using online gas chromatography.

2.5. Electrochemical measurements

Electrochemical measurements were performed on a CHI 660D electrochemical workstation (Shanghai Chenhua, China) using a standard three-electrode cell with a working electrode, a platinum wire as counter electrode, and a standard saturated calomel elec-trode (SCE) in saturated KCl as reference electrode. The working electrodes were prepared by dip-coating: Briefly, 5 mg of photo-catalyst was suspended in 0.1 mL of ethanol in the presence of 1% Nafion to produce slurry, which was then dip-coated onto a 2 cm × 1.5 cm FTO glass electrode and drying at 25 ° C.

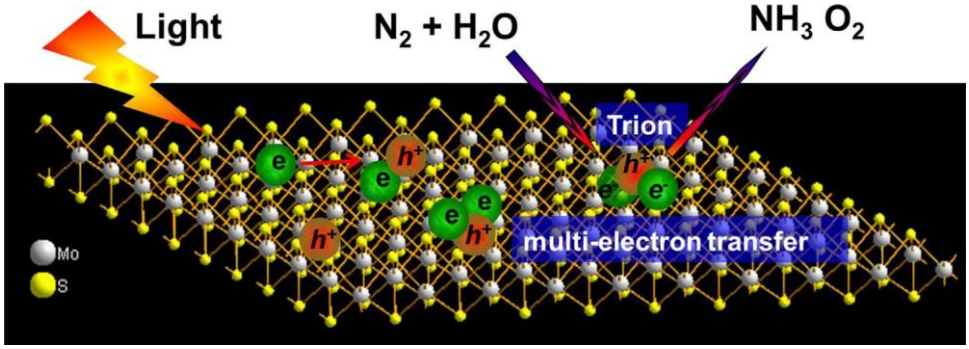

Scheme 1. Schematic illustration of the trion induced multi-electron N_2 reduction process.

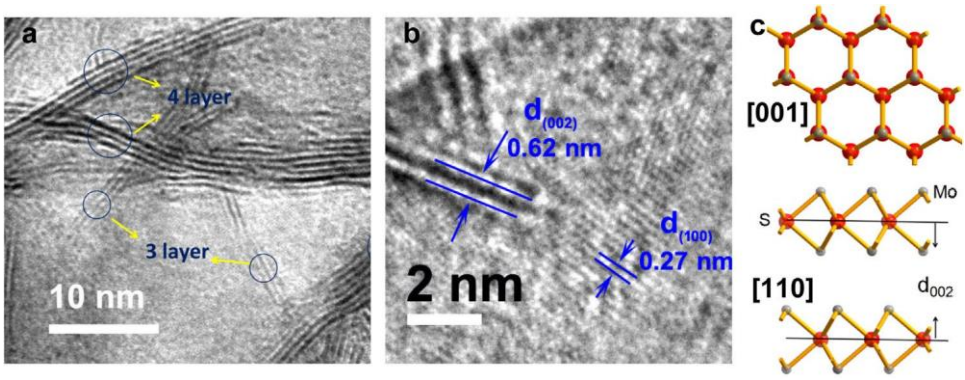

Fig. 1. (a) TEM and (b) HRTEM image of sonicated ultrathin MoS_2 . (c) Schematic illustration of the crystal structure of hexagonal MoS_2 along [001] and [110] directions.

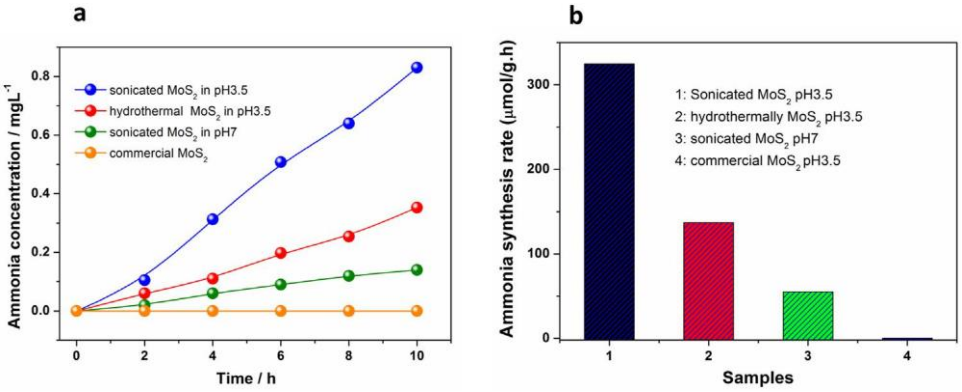

Fig. 2. N_2 reduction and ammonia production efficiency of the as-prepared MoS_2 samples under different conditions. (a) Obtained ammonia concentration at different reaction time. (b) The corresponding ammonia synthesis rate.

2.6. Calculation of electron transfer number

For an adsorption-controlled and irreversible electrode process, according to Laviron [33], Ep is defined by the following equation:

$$Ep = E^0 + (RT/anF)\ln \quad RTK^0/anF \quad RTF/anF \quad \ln$$

where a is transfer coefficient, k^0 is standard rate constant of the reaction, n is electron transfer number involved in the rate-determining step, is scan rate(mV/S), and E^0 is formal potential. Other symbols have their usual meanings. For an irreversible elec-trode process, a ≈ 0.5.

3. Results and discussion

Fig. 1a shows the TEM image of the sonicated ultrathin MoS_2 , which exhibits a lamellar morphology with 3~5 layers of S-Mo-S. The ultrathin structure was further confirmed by an HRTEM image. As shown in Fig. 1b, the interplanar spacing of 0.62 nm and 0.27 nm were clearly observed, which is consistent with the d spac-ing of (002) and (100) planes of hexagonal MoS_2 , respectively. The schematic crystal structure of hexagonal MoS_2 in Fig. 1c further illustrates the lattice structure on (001) plane and the S-Mo-S lay-ered structure along [001] and [110] directions. XRD pattern of the sonicated ultrathin MoS_2 indicates its high crystallinity and purity (Fig. S1). All of the diffraction peaks agree well with the standard pattern of hexagonal MoS_2 (JCPDS card No. 75-1539). The widened diffraction peaks were ascribed to the ultrathin thickness which is about 3.5 nm determined by calculating the full width at half maximum (FWHM) value of the (002) diffraction peak based on the Scherrer equation. ICP analysis indicates the stoichiometry ratio of Mo: S in sonicated ultrathin MoS_2 is 1: 1.75, indicating a large amount of S vacancies may exist in the ultrathin structure. Without the ultrasonic treatment, the thickness of the hydrothermally syn-thesized MoS_2 nanosheet was mainly around 9–14 layers of S-Mo-S (as shown in Fig. S2).

To investigate the photocatalytic N_2 reduction properties of the prepared MoS_2 samples, 15 mg of the as-prepared powder sample was dispersed in 200 mL of deionized water in an open Pyrex cell equipped with a circulating water cooling system to main the reac-tion temperature at 25 ° C. Before that, the ultrathin MoS_2 samples were washed with dilute hydrochloric acid (HCl) many times to eliminate the residual NH_4^+ which may be brought on in the syn-thetic process. During this process, the adsorbed NH_4^+ on the MoS_2 sample was replaced by H^+ via cation exchange. After the HCl wash-ing, no residual NH_4^+ was detected in the reaction solution and the S^{2-} in the reaction solution was decreased to 1.1 mol/L by ion chromatography. The reaction mixture was then irradiated under a 500 W Xenon arc lamp. During this process, the atmospheric N_2 in the reaction system was reduced into NH_4^+ by the ultrathin MoS_2 photocatalyst.

Fig. 2a shows the obtained ammonia concentration for various MoS_2 samples at different reaction conditions. Control experiments showed that NH_4^+ cannot be detected in the absence of MoS_2 cat-alyst or solar light irradiation. In contrast, simulated solar light irradiation resulted in continuous ammonia production from pure water by the as-prepared ultrathin MoS_2 samples. The generated ammonia concentration by the sonicated ultrathin MoS_2 sample is about 0.14 mg/L within 10 h in pure water. In an acidic reaction

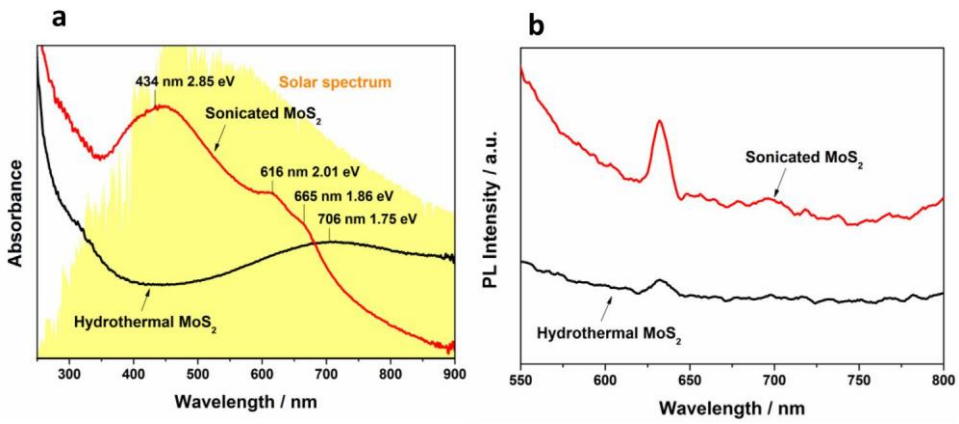

Fig. 3. Optical properties of the as-prepared MoS_2 samples. (a) UV−vis absorption spectra of the as-prepared MoS_2 samples dispersed in pure water. (b) Photoluminescent spectra of the as-prepared MoS_2 samples excited at 420 nm at room temperature.

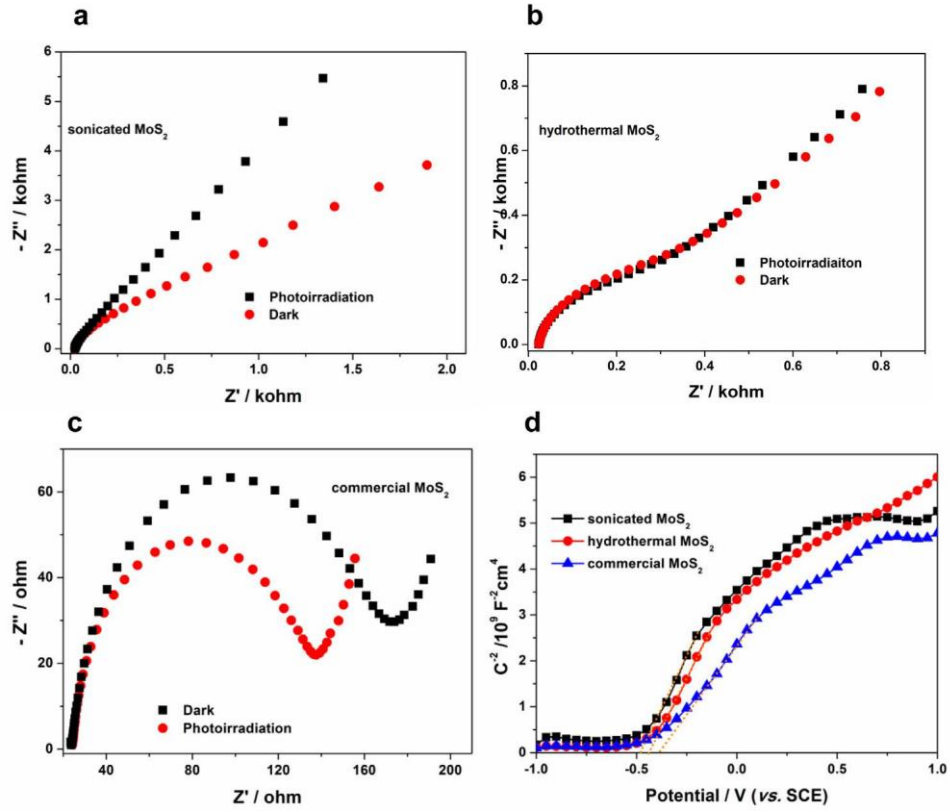

Fig. 4. Electrochemical impedance spectra (EIS) of sonicated ultrathin MoS_2 (a), hydrothermal MoS_2 (b) and commercial MoS_2 (c). (d) Mott−Schottky plots of the synthetic MoS_2 samples and commercial MoS_2 .

solution (pH 3.5) which could provide excess protons to decrease the kinetic barrier for N_2 reduction, the generated ammonia con-centration was increased to 0.83 mg/L by the sonicated ultrathin MoS_2 sample within 10 h, with a high ammonia synthesis rate of about 325 mol/g (catalyst) h (Fig. 2b). Under the same conditions, the generated ammonia concentration by hydrothermally MoS_2 sample is 0.35 mg/L and no ammonia was detected by commer-cial bulk MoS_2 , indicating the unique advantage of ultrathin MoS_2 for photocatalytic N_2 reduction to ammonia. When the photocat-alytic N_2 reduction experiment was conducted under visible light irradiation (> 420 nm), the ultrathin MoS_2 samples also exhibited excellent photocatalytic activity. After 10 h of visible light irradi-ation, the obtained ammonia concentration for the sonicated and hydrothermal MoS_2 samples were 0.5 and 0.26 mg/L at pH 3.5 (as shown in Fig. S3). Besides, the stability of the ultrathin MoS_2 was also investigated. After ten consecutive runs for the N_2 photoreduc-tion experiment, the photocatalytic performance of the sonicated ultrathin MoS_2 was well-maintained and a total of 1.6 mg NH_4^+ was produced after 100 h. The XRD pattern (Fig. S4) and the UV–vis absorption spectrum (Fig. S5) of the spent ultrathin MoS_2 photo-catalyst are almost the same as that of the initial MoS_2 sample, indicating the high stability of ultrathin MoS_2 . The turnover num-ber under this condition is 1.22, indicating the ammonia generation on MoS_2 surface is catalytic. Besides, a considerable amount of O_2 generation was observed during the photocatalytic ammonia syn-thesis process when the N_2 reduction experiment was conducted in a closed reaction system, indicating water may act as the sacrificial electron donor of photogenerated holes for ammonia generation.

To further confirm that the NH_4^+ detected comes from N_2 reduc-tion, we conducted an isotopic labelling study using gaseous N_2 which contains 20 vol% $^{15}N_2$ as the purge gas. Infrared spectroscopy was used to characterize the NH_4^+ product. As shown in Fig. S6, besides the $^{14}NH_4^+$ which has an infrared absorption peak around 1400 cm^{-1}, $^{15}NH_4^+$ was also observed on the infrared spectrum with an adsorption peak around 1351 cm^{-1} which is in good agree-ment with the value estimated according to the isotope effect (that is, 1400 cm^{-1} × $(14/15)^{1/2}$ = 1352 cm^{-1}). This isotope labelling study confirmed that the NH_4^+ detected in our experiments origi-nated from photocatalytic N_2 reduction and not from other sources.

Optical properties were studied to investigate the origin of the solar light induced N_2 photoreduction property of the ultrathin MoS_2 samples. The UV–vis absorption spectrum of the sonicated MoS_2 sample (Fig. 3a) shows the well-known A and B excitonic absorption bands at 665 nm (1.86 eV) and 616 nm (2.01 eV) [34,35]. These two absorption bands have been well established to be the direct excitonic transitions at the K point of the Brillouin zone in monolayer and few-layer MoS_2. In addition, an intense absorp-tion band centered at 434 nm (2.85 eV) was also clearly observed. This is a feature absorption that is universal to monolayer TMDs and associated with Van Hove singularities in the density of states [36]. Different from the sonicated ultrathin MoS_2, the hydrothermal MoS_2 only displays one broad absorption band centered at 706 nm that may be attributed to the mixed optical absorption by the direct and indirect band transitions in few-layer and thicker MoS_2. The hydrothermal and the sonicated MoS_2 samples exhibit the similar photoluminescence (PL) spectrum around ~633 nm (Fig. 3b), cor-responding to a band gap at 1.95 eV. However, the PL intensity of the sonicated MoS_2 is much stronger than that of the hydrother-mal MoS_2 sample. A previous study by Mark et al. has demonstrated the PL around 1.9 eV was originated from the relaxation of direct excitons in monolayer MoS_2 [35]. Both of the UV–vis absorption and PL spectrum indicate the larger amount of photo-generated excitons in the sonicated sample under the same conditions, which may play a vital role in improving the photocatalytic N_2 reduction performance.

Photoelectrochemical measurements on the as-prepared MoS_2 samples further revealed the origin of the solar light induced N_2 reduction property. Fig. 4a shows the electrochemical impedance spectra (EIS) of the sonicated ultrathin MoS_2 electrode under dif-ferent conditions. It is obvious that the diameter of the semicircle loop on the EIS Nynquist plot is enlarged under light irradiation, indicating a much decreased electrical conduction under photoir-radiation. Generally, the conductivity of a semiconductor electrode is increased under light irradiation because of the generation of photo-electrons. The abnormal negative photoconductivity of ultrathin MoS_2 was induced by the strong many-body interactions in ultrathin 2D system, where photoexcited electron-hole pairs join the excess free charges to form trions (bound states of two electrons and one hole) [37]. These charged excitons have an increased car-rier effective mass, substantially diminishing the conductivity. The negative photoconductivity is also slightly observed in hydrother-mal MoS_2 sample (Fig. 4b), and completely vanished in commercial MoS_2 (Fig. 4c). Combined with the above photocatalytic perfor-mance of different MoS_2 samples, it is obvious the photocatalytic N_2 reduction performance is closely related to their photocon-ductivity. Only the hydrothermal and sonicated MoS_2 which have negative photoconductivity exhibited the photocatalytic N_2 reduc-tion activity. Besides, the sonicated ultrathin sample with a much enhanced photoreduction of conductivity possesses the highest photocatalytic activity. The commercial MoS_2 which has normal positive photoconductivity exhibited no N_2 photoreduction per-formance. Therefore, the variation of photoconductivity in different MoS_2 samples is synchronization with the variation of their photo-catalytic activity to a certain extent. This indicates trions induced negative photoconductivity may play an important role on the pho-tocatalytic N_2 reduction performance of ultrathin MoS_2.

To investigate the possibility of trion-induced N_2 photoreduc-tion by ultrathin MoS_2, thermodynamic process of N_2 reduction on various MoS_2 samples was firstly analyzed by electrochem-ical studies. Fig. 4d is Mott−Schottky spectra of different MoS_2 samples, which is usually used for the analysis of the flat band potential (E_{fb}) of semiconductor electrodes [38]. The positive slope of the plot indicates these MoS_2 samples are n-type semiconduc-tor with electrons as the majority charge carriers. The E_{fb} values which were calculated from the intercept of the axis with potential value were at −0.49 V, −0.44 V and −0.38 V vs SCE for the soni-cated, hydrothermal and commercial MoS_2 samples, respectively. For many n-type semiconductors, E_{fb} is considered to be about 0.1 V below the conduction band (E_{cb}) [39]. Based on this, the estimated E_{cb} values of the sonicated, hydrothermal and commercial MoS_2 samples were −0.35 V, −0.3 V and −0.24 V vs. NHE respectively. It is obvious the conduction band edge position for all of the MoS_2 samples is located below the thermodynamic reduction potentials of N_2 /N_2 H and N_2 /NH_3 OH^+, which indicates photogenerated elec-trons on MoS_2 are difficult to take part in the N_2 reduction reaction by one-electron or two-electron transfer process.

It is most likely N_2 reduction to ammonia occurs by a multi-electron transfer process on the MoS_2 surface, considering the lower reduction potentials of N_2 /N_2 H_5^+ and N_2 /NH_3. However, multi-electron transfer process is extremely difficult from a kinetic view. Although it is thermodynamically accessible, commercial MoS_2 exhibited no catalytic activity for ammonia generation. This study indicates the excellent N_2 reduction performance of ultrathin MoS_2 may be ascribed to trions induced multi-electron transfer reduction process. Besides, the valence band edge potentials of the sonicated and hydrothermal ultrathin MoS_2 samples which esti-mated from the band gap and E_{cb} were calculated at 1.51 and 1.45 V vs. NHE respectively at pH 7. These potentials are energetically large enough for water oxidation (0.82 V vs. NHE) at pH 7.

To verify the possibility of multi-electron reduction process on ultrathin MoS_2, the electron transfer number upon N_2 reduction on the as-prepared different MoS_2 electrodes was studied by analyz-ing the variation of the reduction peak potential (E_p) along with the change of the scan rate ( ) in a photoelectrochemical measurement [33]. From the slope of the E_p -ln curve, a six electron transfer pro-cess (n = 6.04, Fig. 5a) was qualified on the ultrathin MoS_2 electrode based on the analysis of its higher reduction peak around −1.17 V vs. SCE. Under the same conditions, the electron transfer number of commercial MoS_2 electrode is calculated to be 2.33 (Fig. 5b). As mentioned above, photogenerated electrons in MoS_2 is energeti-cally impossible for N_2 reduction by two-electron transfer process. Therefore, without trions assistant multi-electron transfer process, commercial MoS_2 is inactive on N_2 photoredution.

Based on the above analysis, the mechanism for the photocat-alytic N_2 reduction on ultrathin MoS_2 was illustrated in Scheme 1. As an n-type semiconductor, ultrathin MoS_2 possess lots of free electrons. Under solar light irradiation, these free electrons were attracted by the light generated excitons (electron-hole pairs) to form charged excitons (trions, as shown in Scheme 1). These charged excitons have multiple electrons in one bound state, which could contribute to multi-electron transfer reactions. First-principles calculations have indicated the valence band maximum and conduction band minimum both in bulk and single layer MoS_2 mainly consists of Mo 4d contributions [40]. Therefore, the photo-generated charged excitons were mainly located around the Mo sites. Due to the large amount of S vacancies in the ultrathin MoS_2, the N_2 molecules are most probably captured by these S vacancies and activated upon donating electrons from its bonding orbitals and accepting electrons to its three antibonding orbitals. From the crystal structure in Fig. 1c, it can be seen every S atom

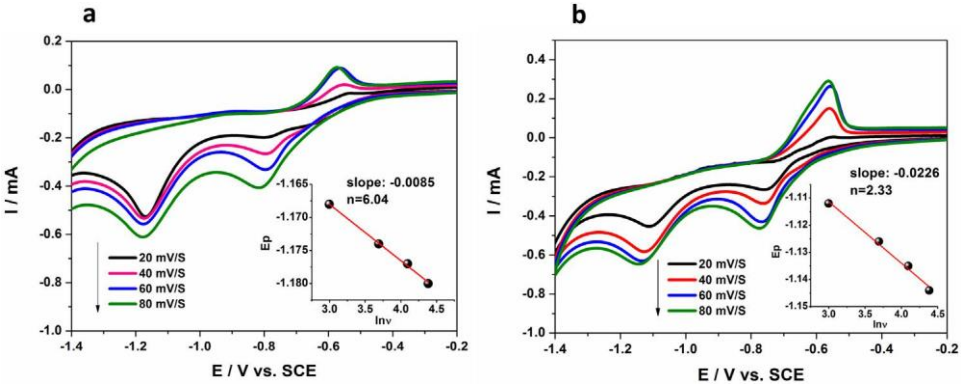

Fig. 5. Kinetic study of N_2 photoreduction on MoS_2 catalyst by photoelectrochemical measurements. (a) Cyclic voltammograms of sonicated ultrathin MoS_2 electrode. (b) Cyclic voltammograms of commercial MoS_2 electrode. The experiment was performed at different scan rates in N_2 saturated 0.5 M Na_2SO_4 (pH = 3.5) under room temperature (25 ° C) and simulated sun light irradiation; Inset: the plot for the reduction peak potential (Ep) vs. ln (scan rate).

connected with three Mo atoms. Therefore, the adsorbed N_2 molecules on the S vacancy are most likely surrounded by three Mo atoms. Under solar light irradiation, the photogenerated charged excitons on these Mo atoms may cooperate with the center-adsorbed N_2 molecule and resulted in a possible trions assistant six-electron reduction process. In our N_2 photoreduction exper-iment, only NH_4^+ was detected, although there are possibilities for the formation of other products such as N_2H_4 in N_2 reduction process. This photocatalytic performance data, therefore, further support our hypothetical interpretations of the N_2 reduction mech-anism.

4. Conclusion

Simultaneous multi-electron reduction of N_2 was put forward to decrease the thermodynamic barrier for N_2 photoreduction to ammonia. Although this process is extremely difficult from a kinetic point, our study indicates it may be realized by electron-rich semiconductor photocatalyst which have high concentration of localized electrons such as trions. Ultrathin MoS_2 was syn-thesized as model material to verify trion induced simultaneous multi-electron photoreduction of N_2 . Photoelectrochemical mea-surements proved trions in ultrathin MoS_2 was responsible for the photocatalytic N_2 reduction performance by simultaneous six-electron reduction process. The photocatalytic ammonia synthesis rate of ultrathin MoS_2 is up to 325 mol/g h without the assistant of any organic scavengers or co-catalyst. Under the same condi-tions, the bulk MoS_2 without charged excitons did not exhibit any N_2 reduction activity. The methodology of simultaneous multi-electron reduction has wide implications for other multi-electron transfer reactions such as CO_2 photoreduction in electron-rich cat-alytic material beyond ultrathin MoS_2 .

Acknowledgments

This work was financially supported by the National Basic Research Program of China (2013CB933200), National Natural Sci-ence Foundation of China (51272269, 51272303, 51472260), and the research grant (16ZR1440800) from Shanghai Science and Technology Commission.

Appendix A. Supplementary data

References

[1] J.A. Pool, E. Lobkovsky, P.J. Chirik, Nature 427 (2004) 527–530.
[2] J.W. Erisman, M.A. Sutton, J. Galloway, Z. Klimont, W. Winiwarter, Nat. Geosci. 1 (2008) 636–639.
[3] H. Tanaka, A. Sasada, T. Kouno, M. Yuki, Y. Miyake, H. Nakanishi, Y. Nishibayashi, K. Yoshizawa, J. Am. Chem. Soc. 133 (2011) 3498–3506.
[4] R. Schlögl, Angew. Chem. Int. Ed. 42 (2003) 2004–2008.
[5] T. Shima, S. Hu, G. Luo, X. Kang, Y. Luo, Z. Hou, Science 340 (2013) 1549–1552.
[6] Y. Tanabe, Y. Nishibayashi, Coordin. Chem. Rev. 257 (2013) 2551–2564.
[7] G.N. Schrauzer, T.D. Guth, J. Am. Chem. Soc. 99 (1977) 7189–7193.
[8] O. Rusina, A. Eremenko, G. Frank, H.P. Strunk, H. Kisch, Angew. Chem. Int. Ed. 40 (2001) 3993–3995.
[9] E. Endoh, J.K. Leland, A.J. Bard, J. Phys. Chem. 90 (1986) 6223–6226.
[10] J. Soria, J.C. Conesa, V. Augugliaro, L. Palmisano, M. Schiavello, A. Sclafani, J. Phys. Chem. 95 (1991) 274–282.
[11] O.P. Linnik, H. Kisch, Mendeleev Commun. 18 (2008) 10–11.
[12] D. Zhu, L. Zhang, R.E. Ruther, R.J. Hamers, Nat. Mater. 12 (2013) 836–841.
[13] K. Tennakone, C.T.K. Thaminimulla, W.C.B. Kiridena, Langmuir 9 (1993) 723–726.
[14] N. Bauer, J. Phys. Chem. 64 (1960) 833—837.
[15] T. Bazhenova, A. Shilov, Coord. Chem. Rev. 144 (1995) 69–145.
[16] C. Willis, R.A. Back, Can. J. Chem. 51 (1973) 3605–3619.
[17] H. Li, J. Shang, Z. Ai, L. Zhang, J. Am. Chem. Soc. 137 (2015) 6393–6399.
[18] M. Kitano, Y. Inoue, Y. Yamazaki, F. Hayashi, S. Kanbara, S. Matsuishi, T. Yokoyama, S.W. Kim, M. Hara, H. Hosono, Nat. Chem. 4 (2012) 934–940.
[19] S. Wu, J.S. Ross, G.B. Liu, G. Aivazian, A. Jones, Z. Fei, W. Zhu, D. Xiao, W. Yao, D. Cobden, X. Xu, Nat. Phys. 9 (2013) 149–153.
[20] K.F. Mak, K. He, J. Shan, T.F. Heinz, Nat. Nanotechnol. 7 (2012) 494–498.
[21] Q. Wang, K. Kalantar-Zadeh, A. Kis, J.N. Coleman, M.S. Strano, Nat. Nanotechnol. 7 (2012) 699–712.
[22] J. Shi, D. Ma, G.F. Han, Y. Zhang, Q. Ji, T. Gao, J. Sun, X. Song, C. Li, Y. Zhang, X.Y. Lang, Y. Zhang, Z. Liu, ACS Nano 8 (2014) 10196–10204.
[23] D.Y. Qiu, F.H. da Jornada, S.G. Louie, Phys. Rev. Lett. 111 (2013) 216805.
[24] K. He, N. Kumar, L. Zhao, Z. Wang, K.F. Mak, H. Zhao, J. Shan, Phys. Rev. Lett. 113 (2014) 026803.
[25] A. Chernikov, T.C. Berkelbach, H.M. Hill, A. Rigosi, Y. Li, O.B. Aslan, D.R. Reichman, M.S. Hybertsen, T.F. Heinz, Phys. Rev. Lett. 113 (2014) 076802.
[26] Z. Ye, T. Cao, K. O'Brien, H. Zhu, X. Yin, Y. Wang, S.G. Louie, X. Zhang, Nature 513 (2014) 214–218.
[27] M.M. Ugeda, A.J. Bradley, S.F. Shi, F.H. da Jornada, Y. Zhang, D.Y. Qiu, W. Ruan, S.K. Mo, Z. Hussain, Z.X. Shen, F. Wang, S.G. Louie, M.F. Crommie, Nature Mater. 13 (2014) 1091–1095.
[28] C.H. Lui, A.J. Frenzel, D.V. Pilon, Y.H. Lee, X. Ling, G.M. Akselrod, J. Kong, N. Gedik, Phys. Rev. Lett. 113 (2014) 166801.
[29] L. Cheng, W. Huang, Q. Gong, C. Liu, Z. Liu, Y. Li, H. Dai, Angew. Chem. Int. Ed. 53 (2014) 7860–7863.
[30] L. Tao, X. Duan, C. Wang, X. Duan, S. Wang, Chem. Commun. 51 (2015) 7470–7473.
[31] J. Xie, J. Zhang, S. Li, F. Grote, X. Zhang, H. Zhang, R. Wang, Y. Lei, B. Pan, Y. Xie, J. Am. Chem. Soc. 135 (2013) 17881–17888.
[32] J. Xie, H. Zhang, S. Li, R. Wang, X. Sun, M. Zhou, J. Zhou, X.W. Lou, Y. Xie, Adv. Mater. 25 (2013) 5807–5813.
[33] E. Laviron, J. Electroanal. Chem. Interfacial Electrochem. 52 (1974) 355–393.
[34] A. Splendiani, L. Sun, Y. Zhang, T. Li, J. Kim, C.Y. Chim, G. Galli, F. Wang, Nano Lett. 10 (2010) 1271–1275.
[35] K.F. Mak, C. Lee, J. Hone, J. Shan, T.F. Heinz, Phys. Rev. Lett. 105 (2010) 136805.
[36] L. Britnell, R.M. Ribeiro, A. Eckmann, R. Jalil, B.D. Belle, A. Mishchenko, Y.J. Kim, R.V. Gorbachev, T. Georgiou, S.V. Morozov, A.N. Grigorenko, A.K. Geim, C. Casiraghi, A.H. Castro Neto, K.S. Novoselov, Science 340 (2013) 1311–1314.

[37] K.F. Mak, K. He, C. Lee, G.H. Lee, J. Hone, T.F. Heinz, J. Shan, Nature Mater. 12 (2013) 207–211.
[38] A. Watanabe, H. Kozuka, J. Phys. Chem. B 107 (2003) 12713–12720.
[39] Y. Matsumoto, J. Solid State Chem. 126 (1996) 227–234.
[40] E.S. Kadantsev, P. Hawrylak, Solid State Commun. 152 (2012) 909–913.